Two independent evolutionary routes to Na^+/H^+ co-transport function in membrane pyrophosphatases

Erika Nordbo*, Heidi H. Luoto*, Alexander A. Baykov†, Reijo Lahti* and Anssi M. Malinen*[1]

*Department of Biochemistry, University of Turku, FIN-20014 Turku, Finland.
†Belozersky Institute of Physico-Chemical Biology, Lomonosov Moscow State University, Moscow 119899, Russia.

[1]To whom correspondence should be addressed (email: anssi.malinen@utu.fi).

ABSTRACT

Membrane-bound pyrophosphatases (mPPases) hydrolyze pyrophosphate (PP_i) to transport H^+, Na^+ or both and help organisms to cope with stress conditions, such as high salinity or limiting nutrients. Recent elucidation of mPPase structure and identification of subfamilies that have fully or partially switched from Na^+ to H^+ pumping have established mPPases as versatile models for studying the principles governing the mechanism, specificity and evolution of cation transporters. In this study, we constructed an accurate phylogenetic map of the interface of Na^+-transporting PPases (Na^+-PPases) and Na^+- and H^+-transporting PPases (Na^+,H^+-PPases), which guided our experimental exploration of the variations in PP_i hydrolysis and ion transport activities during evolution. Surprisingly, we identified two mPPase lineages that independently acquired physiologically significant Na^+ and H^+ co-transport function. Na^+,H^+-PPases of the first lineage transport H^+ over an extended [Na^+] range, but progressively lose H^+ transport efficiency at high [Na^+]. In contrast, H^+-transport by Na^+,H^+-PPases of the second lineage are not inhibited by up to 100 mM Na^+. With the identification of Na^+,H^+-PPase subtypes, the mPPases protein superfamily appears as a continuum ranging from monospecific Na^+ transporters to transporters with tunable levels of Na^+ and H^+ co-transport and further to monospecific H^+ transporters. Our results lend credence to the concept that Na^+ and H^+ are transported by similar mechanisms, allowing the relative efficiencies of Na^+ and H^+ transport to be modulated by minor changes in protein structure during the course of adaptation to a changing environment.

SUMMARY STATEMENT

Membrane-bound pyrophosphatases (mPPases) couple PP_i hydrolysis to Na^+ and/or H^+ transport. We report here that the acquisition of physiologically significant Na^+ and H^+ co-transport function has occurred twice within the mPPase protein family during the course of its evolution.

SHORT TITLE: Na^+- and H^+-transporting membrane pyrophosphatases

Key words: membrane transport, proton transport, sodium transport, protein evolution, pyrophosphatase

Abbreviations: ACMA, 9-amino-6-chloro-2-methoxyacridine; AMDP, aminomethylenediphosphonate; IMVs, inverted membrane vesicles; mPPase, membrane-bound PPase; PPase, pyrophosphatase; PP_i, inorganic pyrophosphate; TMA, tetramethylammonium.

INTRODUCTION

Membrane-bound pyrophosphatases (mPPases), which are present in plants, bacteria, archaea and protists, hydrolyze pyrophosphate, a ubiquitous metabolic byproduct, to transport H^+, Na^+ or both across various biological membranes (see references [1–8] for reviews). H^+-transporting mPPases (H^+-PPases) and ATPases operate jointly to maintain the acidic interior of cellular organelles, such as vacuoles in plants and acidocalcisomes in protists and bacteria. In prokaryotes, mPPases additionally localize to the cell membrane, allowing mPPase-mediated [Na^+] and [H^+] gradients to maintain cytoplasmic ion balances and even power ATP synthesis [9,10]. mPPase function is particularly important under stress conditions [3,11], where the efficiency of ATP- or redox-powered ion pumping is diminished. The ability of H^+-PPases to back up cellular energy production and ion pumping has been applied to engineer plants that are resistant to stress conditions, such as dryness, cold and salinity [12–14]. In other cases, the predominant driver of excessive plant growth appears to be the PP_i-hydrolyzing function of H^+-PPases [15]. Notably, mPPases are present in several pathogenic protists, such as *Plasmodium falciparum* and *Trypanosoma cruzi*, and pathogenic bacteria, such as *Bacteroides fragilis* and *Clostridium tetani*, but are absent in humans. Thus, mPPases are potential targets for antimicrobials [16,17].

Structurally, mPPases are among the simplest primary ion transporters and are not evolutionarily (phylogenetically) related to other proteins [18,19]. Functional mPPases are a dimer of two identical, largely hydrophobic polypeptides. Each subunit, comprising 600–900 amino acid residues, typically folds into 16 long α-helices that span the membrane and protrude into the cytoplasm. Each subunit forms a funnel-like structure that integrates the PP_i hydrolysis site at the cytoplasmic end and ion-conductance channel, gate and exit channel at the opposite end [2]. All mPPases apparently share the same core structure and mechanism, whereas poorly understood structural differences in specific enzyme lineages govern the functional divergence of mPPases.

The mPPase superfamily is divided into three phylogenetically and functionally distinct families (Figure 1A). All families share a requirement for Mg^{2+} as an essential cofactor. Canonical K^+-independent H^+-PPases [20] and divergent Na^+-regulated H^+-PPases [21] specifically transport H^+ and require no alkali earth metal ion for activity. The two families are distinct, as reflected in their separation by a very long phylogenetic distance and the fact that Na^+ ions regulate only the divergent H^+-PPases [21]. mPPases of the K^+-dependent family additionally require the binding of K^+ [22] in close proximity to the PP_i hydrolysis site [18,19]. K^+-dependent mPPases are further classified into several subfamilies based on their ion transport specificity. Na^+-transporting PPases (Na^+-PPases) constitute the monophyletic core and are a probable ancestral form of the K^+-dependent family [23]. Recent studies have identified four independent adaptations to H^+-transport activity within the K^+-dependent subfamily. Three evolutionarily independent lineages have created the subfamilies *Carboxydothermus hydrogenoformans*-type, *Flavobacterium johnsoniae*-type and plant-type H^+-PPases, all of which are strictly specific H^+ transporters [23]. In contrast, Na^+- and H^+-transporting PPases (Na^+,H^+-PPases), constituting the fourth evolutionary lineage simultaneously transport Na^+ and H^+ ions with little or no competition between them [24]. The surprisingly frequent emergence of H^+-pumping function within the K^+-dependent family was recently explained by the observation of weak H^+ pumping by Na^+-PPases at sub-physiological Na^+ concentrations (<10 mM) [25]. The acquisition of physiologically significant H^+ pumping thus did not depend on a *de novo* development of a H^+ transport mechanism, but rather on amplification of the pre-existing H^+-pumping function.

In this study, we performed extensive bioinformatic and functional mapping of the phylogenetic/structural space at the interface of Na^+,H^+-PPases and Na^+-PPases. Surprisingly, our data suggest that physiologically significant H^+ and Na^+ co-transport function independently evolved in two closely related mPPase lineages. The lineages differed in the response of their H^+-transport activity to increasing Na^+ concentration in the range of 0.5–100 mM: in one lineage (true Na^+,H^+-PPases), the activity progressively increased, whereas in the other (Na^+-regulated Na^+,H^+,-

PPases), it decreased. Our results reinforce the overall plasticity of the mPPase ion transport mechanism and demonstrate that only minor modifications in the protein structure are required to tune the transport specificity of Na^+-PPases towards H^+.

EXPERIMENTAL

Expression of recombinant mPPases

The full reading frames of 10 bacterial mPPase genes (Table 1) were expressed in *Escherichia coli* C41(DE3) cells using a previously established workflow [23,26]. Unless otherwise specified in Table 1, the template for cloning of the mPPase gene was genomic DNA of the host bacterium obtained from Leibniz-Institute DSMZ (Deutsche Sammlung von Microorganismen und Zellkulturen GmbH). The putative mPPase genes were amplified from genomic DNA using Phusion DNA polymerase (Thermo Scientific). PCR primers introduced *Nde*I and *Xho*I restriction sites at the beginning and end of the gene, respectively, to facilitate cloning of the genes under the control of the isopropyl β-thiogalactopyranoside (IPTG)-inducible T7 promoter in the pET36b plasmid (Novagen). In the cases of Ma-PPase and Cyf-PPase, an *Nde*I restriction site within the reading frame was removed before cloning into pET36b. None of the above DNA modifications changed the translated mPPase reading frame. In the case of Cp-PPase, three inherent *Nde*I sites made the use of this restriction enzyme impractical. Instead, we cloned the gene into the pET15b vector using *Nco*I and *Bam*HI sites. Because genomic DNAs of *Kuenenia stuttgartiensis* and *Dehalogenimonas lykanthroporepellens* were unavailable to us, we inserted synthetic codon-optimized mPPase genes (synthesized by Eurofins Genomics) into pET36b using *Nde*I and *Xho*I restriction sites. The mPPase gene-containing part of each final expression plasmid was verified by DNA sequencing.

mPPase genes were expressed in *E. coli,* and mPPase-containing inverted membrane vesicles (IMVs) were isolated using a published protocol [26]. IMVs were suspended in storage buffer (10 mM Mops-TMA hydroxide pH 7.2, 1 mM $MgCl_2$, 0.9 M sucrose, 5 mM dithiothreitol, and 50 μM EGTA), frozen in liquid N_2, and stored at -85 °C. IMVs were quantified based on their protein content, measured using a Bradford assay [27].

mPPase expression was confirmed by Western analysis as previously described [25]. In short, 10 μg of IMV proteins were separated by SDS-PAGE on 4–20% gradient gels (Thermo Scientific) and blotted onto a nitrocellulose membrane. The membrane was successively treated with 5% (w/vol) nonfat milk, anti-mPPase antibody and fluorescently labeled anti-rabbit secondary antibody [IRDye 800CW Donkey Anti-Rabbit IgG (H + L) Highly Cross Adsorbed (Li-Cor)]. The membrane was scanned and mPPases detected using an Odyssey infrared imager (Li-Cor).

Phylogenetic analysis

The position of Na^+,H^+-PPases within the mPPase superfamily was previously defined by phylogenetic analysis [24]. To construct a more refined phylogenetic tree of the Na^+-PPase and Na^+,H^+-PPase interface, we used the Na^+,H^+-PPase protein sequence from *Bacteroides vulgatus* (NCBI GenBank accession number: WP005846125) as a query in a BLAST search [28] of the NCBI protein sequence database. On the basis of preliminary analyses, full-length sequences located either within the Na^+,H^+-PPase subfamily or occupying nearby Na^+-PPase branches were aligned with MUSCLE 3.6 using default settings [29]. Manually removing redundant sequences, indels and ambiguously aligned residues yielded a sequence block consisting of 101 taxa and 608 amino acid residue columns. The block was used as input for MrBayes 3.1.2 program [30] to calculate the phylogenetic tree. Two parallel runs, each with four Markov chain Monte Carlo chains, were calculated for 10 million generations at a temp setting of 0.2. A sample tree was saved for every 1000 chains, and a single consensus tree was summarized from the resulting sample trees using 25% of the samples as burn-in. The parallel runs converged well, with an average standard deviation of split frequencies of 0.010.

PP_i hydrolysis measurements

The PP_i hydrolysis reaction was continuously recorded at 25 °C using an automatic phosphate analyzer [31]. The reaction vessel (25 ml) contained 0.1 M Mops-TMA hydroxide (pH 7.2), 5.3 mM $MgCl_2$, 160 μM TMA_4PP_i, 40 μM EGTA and specified concentrations of NaCl and KCl. The reaction was initiated by adding IMVs. Reaction rates were calculated from the initial slopes of the P_i liberation traces, and are expressed as mean values ± standard deviation (SD). The results of duplicate measurements were usually consistent within 10%.

Cation transport measurements

Na^+ ion transport into IMVs was determined using ^{22}Na as a tracer [23,32]. The reaction mixture (80 μl) typically contained 0.1 M Mops-TMA hydroxide (pH 7.2), 160 mM TMA chloride, 25 mM K_2SO_4, 5 mM $MgSO_4$, 0.5 mM Na_2SO_4, 40 μM EGTA and 1 mg/ml IMVs. PP_i was not added to control samples. The mixture was supplemented with 2–5 μCi of carrier-free $^{22}NaCl$ (Perkin-Elmer Life Sciences) and incubated for 30 min at 22°C. mPPase activity was initiated by adding 1 mM TMA-PP_i, and the reaction was allowed to continue for 1 min before stopping by chelating free Mg^{2+} with 20 mM EDTA. A 60-μl aliquot of the mixture was immediately filtered through a nitrocellulose membrane (0.2 μm pore size, 13 mm diameter; Millipore), and the externally bound $^{22}Na^+$ was rinsed off with 1 ml of wash buffer (5 mM Mops–TMA hydroxide pH 7.2, 160 mM TMA chloride, 50 mM Na_2SO_4, 0.5 mM $MgSO_4$, and 2 μM EGTA). The membrane was transferred to a microcentrifuge tube and immersed into 1 ml of Ultima Gold scintillation liquid (PerkinElmer Life Sciences). The amount of $^{22}Na^+$ inside the vesicles was determined using a 1215 Rackbeta liquid scintillation counter (LKB-Wallac).

H^+ transport into IMVs was assayed with the pH-sensitive fluorescent dye, 9-amino-6-chloro-2-methoxyacridine (ACMA) [33]. The reaction mixture (2 ml total volume) typically contained 0.15 mg/ml IMVs in 20 mM Mops-TMA hydroxide (pH 7.2), 50 mM KCl, 5.8 mM $MgCl_2$, 8 μM EGTA, 2 μM ACMA and 0.1–100 mM NaCl. Total chloride concentration was maintained at 160 mM by adding TMA chloride. The reaction mixture was incubated for 6 min at 25 °C in a spectrofluorometer (LS-55; Perkin Elmer) before mPPase activity was initiated by adding 475 μM TMA-PP_i. Excitation and emission wavelengths were 428 and 475 nm, respectively.

RESULTS

A phylogenetic analysis divides Na^+,H^+-PPases into clades

A previous analysis [24] placed Na^+,H^+-PPases into a single clade that branches from the main mPPase tree near the experimentally characterized Na^+-PPase of *Methanosarcina mazei* (M in Figure 1A). To determine the evolutionary origin, functional divergence and prevalence of Na^+,H^+-PPases, we created a detailed phylogenetic tree from mPPase protein sequences that represent the structural divergence of Na^+,H^+-PPases and their neighboring Na^+-PPases (Figure 1B). Importantly, phylogenetic analyses performed using different sequence sets or software settings, or an entirely different algorithm (RAxML; Figure S1), produced qualitatively similar results. The distribution of the previously characterized Na^+,H^+-PPases [24] in the resulting trees revealed several functionally uncharted clades. On the basis of trees in Figures 1B and S1, we selected several new mPPases that located to the interface of Na^+-PPases and Na^+,H^+-PPases for functional characterization.

Production of recombinant mPPases

The selected mPPase genes were cloned from genomic DNA of the respective bacteria and expressed in *E. coli* following a published protocol [23,26]. *E. coli* does not have its own mPPase and thus represents a convenient expression host for prokaryotic mPPases. To verify successful recombinant mPPase production, we disrupted *E. coli* cells with a French press and isolated the inverted membrane vesicles (IMVs). Western analysis using a polyclonal antibody previously raised

against a conserved mPPase peptide (IYTKAADVGADLVGKVE) , partially overlapping with the catalytic site, revealed protein bands within the expected mPPase size range (Figure 2A). Importantly, no immunoreactive bands were detected in IMVs isolated from *E. coli* transformed with the cloning vector only.

We also visually assessed the total protein content of IMVs by SDS-PAGE followed by Coomassie staining (Figure 2B). Bands attributable to mPPase exhibited a mobility similar to that of the 60-kDa molecular mass marker; thus, they migrated faster than expected for a 70−84-kDa protein, a common property of membrane proteins, including mPPases [34]. The expression level of mPPases varied depending on the specific protein, but was always less than 10% of total IMV proteins, consistent with previous reports [21,32]. mPPase band intensities obtained using antibody and Coomassie detection correlated reasonably well. The lower-than-expected Western-to-Coomassie intensity ratio of Dl-PPase may indicate lower affinity of the antibody for this protein, which has Thr instead of Val in the eighth position in the above antibody-reactive peptide sequence.

Enzyme activity measurements indicated that all mPPase-containing IMVs exhibited significant PP_i hydrolysis activity, which was absent in IMVs prepared from *E. coli* transformed with the cloning vector only (Figure 2C). The PP_i hydrolysis activities were almost completely insensitive to fluoride, a strong inhibitor of soluble *E. coli* PPase, but were significantly attenuated by aminomethylenediphosphonate (AMDP), an mPPase-specific inhibitor [35]. We therefore conclude that all 10 mPPases selected for characterization of the Na^+-PPase/Na^+,H^+-PPase interface in the phylogenetic tree were expressed as functional recombinant proteins in *E. coli*.

The hydrolytic activity of all novel mPPases typically depends on alkali metal ions

Unlike H^+-PPases, all Na^+-transporting mPPases require Na^+ for enzymatic activity. K^+ further modulates the activity of Na^+-PPases and Na^+,H^+-PPases, whereas both K^+-dependent and K^+-independent H^+-PPases are known. To investigate the role of Na^+ and K^+ as activators of the new mPPases, we determined their PP_i hydrolysis activities over an extended [Na^+] range in the presence and absence of K^+. As depicted in Figure 3, the PP_i hydrolysis activities of the new mPPases, measured at a saturating PP_i concentration, generally showed a bell-shaped dependence on [Na^+]. K^+ modulated the function of all tested mPPases by increasing both their maximal catalytic activity and Na^+-binding affinity, thereby shifting the maximum to the physiological Na^+ concentration range (5–10 mM). The Na^+ and K^+ dependencies of the new mPPases are thus typical of Na^+-PPases [32] or Na^+,H^+-PPases [24], but not of H^+-PPases [36,21,37].

Modeling the Na^+ dependencies of PP_i hydrolysis rates (v) using Equation 1 yielded the parameter values shown in Table 2. The equation was derived for Scheme 1, which assumes activating and inhibiting Na^+ binding sites on mPPase, characterized by the dissociation constants K_a and K_i, respectively. The value of activity for the reaction in the presence of K^+ (V_2) was set to the value of activity measured in the absence of K^+ (V_1), assuming that K^+ and the inhibiting Na^+ compete for the same site on the enzyme. The V_2 value for the reaction without K^+ was assumed to be zero simply to account for the small decrease in activity at high [Na^+] observed for some enzymes. Accordingly, the K_i value estimated for the K^+-lacking reaction is not physically meaningful. Parameter a in Equation 1 refers to soluble *E. coli* PPase background, which had a value of 0.010 ± 0.006 $\mu mol \cdot min^{-1} \cdot mg^{-1}$ and was mPPase-independent. The parameter values in Table 2 indicate that K^+ increased the maximal activity (V_1) 1.4–4.1-fold and decreased the binding constant for the activating Na^+ ion (K_a) 19–210-fold. The only exception was Ma-PPase, where K^+ slightly decreased rather than increased V_1.

$$v = (V_1 + V_2[Na^+]/K_i)/(1 + K_a/[Na^+] + [Na^+]/K_i) + a \quad \text{(Eq. 1)}$$

$$\begin{array}{ccccc} & \overset{K_a}{} & & \overset{K_i}{} & \\ ES & \leftrightarrow & ESNa & \leftrightarrow & ESNa_2 \\ & & \downarrow V_1 & & \downarrow V_2 \end{array}$$

Scheme 1 Na^+ binding to the enzyme–substrate complex

All novel mPPases can transport Na^+ and H^+

mPPase-mediated Na^+-transport activity resulted in PP_i-dependent accumulation of $^{22}Na^+$ in IMVs (Figure 4). The previously characterized H^+-PPase of *Leptospira biflexa* (Lb-PPase) and Na^+-PPase of *Chlorobium limicola* (Cl-PPase) [23] served as negative and positive controls, respectively. After the addition of PP_i, the level of Na^+ inside IMVs harboring the new mPPases increased at least 6-fold, whereas there was no increase in [Na^+] in Lb-PPase IMVs. Overall, the level of Na^+ accumulation in IMVs harboring the new mPPases was comparable to that in Cl-PPase IMVs. We conclude that all new mPPases possess Na^+ transport activity that is comparable to that of previously characterized Na^+-transporting PPases.

mPPase-mediated H^+ transport was assayed using ACMA [33], whose fluorescence is quenched upon acidification of the IMV lumen. Typical of all known Na^+-transporting mPPase types, all new mPPases also exhibited significant H^+-transport rates at low Na^+ concentrations (Figure 5A).

Two Na^+,H^+-PPase clades differ in the sensitivity of their H^+ transport activity to Na^+

As previously reported [25], the intrinsic H^+-transport activity of Na^+-PPases is lost at Na^+ concentrations above 5–10 mM, whereas Na^+,H^+-PPases and H^+-PPases maintain their H^+ transport activity in the presence of up to 100 mM Na^+. The results shown in Figure 5A indicate that the novel mPPases can be divided into three groups based on the response of their H^+-pumping activities to Na^+. Bm-, Dl-, Ks-, Mme-, Ov- and Ss-PPases are clearly Na^+-PPases because these enzymes mediated moderate H^+ transport that completely disappeared at 5–10 mM [Na^+]. The second group includes Mr- and Cyf-PPases, whose H^+-transport activities increased with increasing [Na^+] up to 100 mM, identifying them as members of the previously described Na^+,H^+-PPase subfamily [24]. Finally, Ma- and Cp-PPases maintained H^+ transport activity in the presence of 10 mM Na^+, but eventually suffered progressive loss of activity at higher [Na^+], the effect being less pronounced with Ma-PPase. We therefore categorize this novel subfamily of mPPases as Na^+-regulated Na^+,H^+-PPases.

The identification of the latter subfamily prompted us to re-evaluate the H^+-transport activities of five previously reported Na^+,H^+-PPases that were defined as such based on their ability to transport H^+ under physiological conditions, namely in the presence of >10 mM Na^+ [24]. As Figure 5B makes clear, mPPases from *Clostridium lentocellum* (Clen-PPase) and *Clostridium leptum* (Clep-PPase) lost their H^+-transport efficiency at high [Na^+] and therefore belong to Na^+-regulated Na^+,H^+-PPases. In contrast, mPPases from *Akkermansia muciniphila* (Am-PPase), *B. vulgatus* (Bv-PPase) and *Prevotella oralis* (Po-PPase) maintained strong H^+ transport activity at all tested [Na^+] and are therefore true Na^+,H^+-PPases. These results reinforce the existence of two functionally distinct Na^+,H^+-PPase subtypes.

DISCUSSION

Characterization of the enzymatic and transport activities of mPPases that occupy a position in the protein phylogenetic tree close to or within the previously identified Na^+,H^+-PPase subfamily revealed the presence of two types of Na^+/H^+ co-transporting mPPases. Both transporter types mediated significant H^+ pumping at physiological Na^+ concentrations (5–10 mM) and hence differ from Na^+-PPases, which do not transport H^+ in these conditions. However, for some Na^+,H^+-PPases, namely those regulated by Na^+, H^+-transport activity was progressively tuned down at 10–

100 mM Na^+, whereas the "true" Na^+,H^+-PPases retained their full H^+-pumping efficiency at high [Na^+]. The mPPase phylogenetic tree in Figure 1B indicates that the Na^+-regulated Na^+,H^+-PPases specifically occupy clades descending from node A in the tree, whereas the true Na^+,H^+-PPases segregate into clades that descend from node B. The fact that multiple experimentally characterized Na^+-PPases occupy branches between the true and Na^+-regulated Na^+,H^+-PPases indicates that the two Na^+,H^+-PPase types do not lie directly on the same evolutionary pathway. Importantly, two entirely different algorithms (MrBayes and RAxML) produced very similar trees (Figures 1B and S1). The functional data and phylogenetic analyses thus converge on a model that includes two independent, adaptive evolutionary pathways from Na^+-PPase ancestors to physiologically significant Na^+/H^+ co-transporters. The similarity of Na^+ and K^+ dependencies indicates that the mechanisms that modulate ion binding and activity have not significantly changed during the divergent evolution of Na^+-PPases to Na^+,H^+-PPases.

The discovery of two independent acquisitions of physiologically significant Na^+ and H^+ co-transport function reinforces the plasticity of mPPase ion transport activity. The plasticity and adaptability of transport specificity appears to be particularly prevalent within the K^+-dependent mPPase subfamily, whose evolutionary history records three or four independent adaptations from Na^+-PPase to H^+-PPase [1,21], in addition to the two Na^+-PPase→Na^+,H^+-PPase lineages described in this study. Because mPPases are regarded as ancient enzymes [20], their trend-like adaptive evolution from Na^+ pumping to H^+ pumping provides significant experimental support for the "Na^+-first" hypothesis [38,39], which posits that primordial biological membranes employed Na^+ as the coupling ion, at least in part, because these membranes were still permeant to H^+. Membrane evolution to an H^+-tight variant accompanied increasing sophistication of life forms, and selective pressure began to favor the energetically more efficient H^+ coupling in membrane bioenergetics. The adaptation of Na^+-PPases to H^+ pumping may have been particularly favored because their inherent promiscuity already allowed H^+ pumping at sub-physiological Na^+ concentrations [25].

On a molecular level, at least two evolutionary pathways leading to monospecific H^+ pumping appear to involve relocation of a specific Glu residue in the ion transport channel [23]. This Glu residue appears to participate in Na^+ binding in Na^+-PPases and is part of the channel gate [2]. Its relocation along the same transmembrane α-helix or to a neighboring α-helix may modify the ion-binding selectivity of the channel towards H^+ [25]. However, sequence comparisons have failed to identify a conservation pattern of Glu or other residues lining the ion-transport channel in the Na^+-regulated and true Na^+,H^+-PPases that correlates with transport specificity. It therefore appears that functional differences between Na^+,H^+-PPases and Na^+-PPases are not dictated by the simple acquisition of few key residues. We previously suggested that an Asp residue (Asp-146 in *B. vulgatus* Na^+,H^+-PPase) together with three closely neighboring residues, all located outside the ion conductance channel [24], constitute the key motif for acquisition of the Na^+/H^+ co-transport function [24]. However, our new data revealed this motif in several Na^+-PPases, namely Ks-, Bm-, Ks-, Ov- and Ss-PPase, suggesting that the functional significance of the Asp motif was previously overestimated. It now seems that, because the transport mechanism of Na^+-PPases is only marginally H^+ excluding, combinations of small changes at the amino acid level could readily modify mPPase tertiary structure, causing the H^+ exclusion mechanism to lose its efficiency and converting Na^+-PPase into the Na^+/H^+ co-transport mode. Indeed, molecular dynamics simulations of the ATP synthase rotor predict that subtle variations in the geometry and conformational dynamics of two ion-binding sites of similar chemical makeup can significantly contribute to differentiating their Na^+/H^+ selectivity [40].

Canonical Na^+-PPases can transport both Na^+ and H^+ at low (< 10 mM) [Na^+], but only Na^+ at higher [Na^+] [25]. The Na^+-binding site responsible for the inhibition of H^+ transport is different from that involved in transporter activation in both PP_i hydrolysis and cation transport because the latter site is saturated at much lower [Na^+]. We previously argued that the former site (designated N/H) is located close to the gate and can accept either Na^+ or the proton released from the

nucleophilic water molecule during its attack on PP_i, whereas the latter site (designated N) binds Na^+ transiently en route to the N/H site [25]. In the framework of this hypothesis, the difference between Na^+-PPases, Na^+-regulated Na^+,H^+-PPases and true Na^+,H^+-PPases may lie in the affinity of the N site for Na^+. Alternatively, an allostery model can be proposed in which binding of H^+ or Na^+ to one subunit of a dimeric mPPase elicits structural changes in the other subunit, allowing it to bind and transport, more or less preferentially, the alternative ion [24]. Accordingly, the N and N/H sites may be the same, but allosterically modified, sites in different subunits, and the difference between all Na^+-transporting mPPase types may be attributable to the size of the allosteric effect. Determining the three-dimentional structure of Na^+,H^+-PPase with bound Na^+ ions would be a great asset to distinguishing between these possibilities. The available structures of Na^+-PPase [19] are of a limited value in this respect as they contain no bound Na^+. Notably, the much lower affinity of the site responsible for the small inhibition of PP_i hydrolysis by Na^+ in all Na^+-transporting mPPases (Figure 4; see also References [23–26,41]) indicates that this site is different from the N/H and N sites.

In conclusion, membrane PPases display remarkable functional divergence with respect to transport specificity and ligand requirements. Because this protein family is amenable to structural studies and is relatively simple to manipulate, it constitutes an attractive model system for deciphering the general principles governing the mechanism, specificity and evolution of chemically fueled primary ion pumps. Furthermore, H^+-PPases are well-recognized for their ability to improve stress resistance when overexpressed in agricultural plants [42].The newly discovered Na^+,H^+-PPase subtypes therefore provide further unexplored opportunities in plant engineering.

ACKNOWLEDGEMENTS

We thank Risto Jokinen for skillful technical assistance and the CSC–IT Center for Science for the computational resources used in the phylogenetic analysis.

DECLARATION OF INTERESTS

The authors declare no conflicts of interest.

FUNDING

This work was supported by grants from the Academy of Finland (139031), the Russian Foundation for Basic Research (15-04-0482815), and the Ministry of Education and the Academy of Finland (to the National Graduate School in Informational and Structural Biology). A.M.M. was additionally supported by the Instrufoundation (Instrumentariumin tiedesäätiö) and the Finnish cultural foundation (Suomen Kulttuurirahasto). H.H.L was additionally supported by the Emil Aaltonen foundation (Emil Aaltosen säätiö) and Turku University foundation (Turun Yliopistosäätiö).

AUTHOR CONTRIBUTION

E.N. and H.H.L. performed the experiments. E.N. performed the phylogenetic analysis. All authors were involved in designing the study, interpreting the results and writing the manuscript.

REFERENCES

1 Baykov, A.A., Malinen, A.M., Luoto, H.H. and Lahti, R. (2013) Pyrophosphate-fueled Na^+ and H^+ transport in prokaryotes. Microbiol. Mol. Biol. Rev. **77**, 267–276

2 Tsai, J.-Y., Kellosalo, J., Sun, Y.-J. and Goldman, A. (2014) Proton/sodium pumping pyrophosphatases: the last of the primary ion pumps. Curr. Opin. Struct. Biol. **27**, 38–47

3 Serrano, A., Perez-Castineira, J.R., Baltscheffsky, M. and Baltscheffsky, H. (2007) H^+-

PPases: yesterday, today and tomorrow. IUBMB Life **59**, 76–83

4 Drozdowicz, Y.M. and Rea, P.A. (2001) Vacuolar H(+) pyrophosphatases: from the evolutionary backwaters into the mainstream. Trends Plant Sci. **6**, 206–211

5 Maeshima, M. (2000) Vacuolar H(+)-pyrophosphatase. Biochim Biophys Acta **1465**, 37–51

6 Lander, N., Cordeiro, C., Huang, G. and Docampo, R. (2016) Polyphosphate and acidocalcisomes. Biochem. Soc. Trans. **44**, 1–6

7 Gaxiola, R.A., Palmgren, M.G. and Schumacher, K. (2007) Plant proton pumps. FEBS Lett. **581**, 2204–2214

8 Martinoia, E., Maeshima, M. and Neuhaus, H.E. (2007) Vacuolar transporters and their essential role in plant metabolism. J Exp. Bot. **58**, 83–102

9 Baltscheffsky, H., Von Stedingk, L.V, Heldt, H.W. and Klingenberg, M. (1966) Inorganic pyrophosphate: formation in bacterial photophosphorylation. Science **153**, 1120–1122

10 Baltscheffsky, M. (1967) Inorganic pyrophosphate and ATP as energy donors in chromatophores from *Rhodospirillum rubrum*. Nature **216**, 241–243

11 Hernández, A., Herrera-Palau, R., Madroñal, J.M., Albi, T., López-Lluch, G., Perez-Castiñeira, J.R., Navas, P., Valverde, F. and Serrano, A. (2016) Vacuolar H(+)-pyrophosphatase AVP1 is involved in amine fungicide tolerance in *Arabidopsis thaliana* and provides tridemorph resistance in yeast. Front. Plant Sci. **7**, 85

12 Gaxiola, R. A., Li, J., Undurraga, S., Dang, L. M., Allen, G. J., Alper, S. L. and Fink, G. R. (2001) Drought- and salt-tolerant plants result from overexpression of the AVP1 H^+-pump. Proc. Natl. Acad. Sci. U.S.A. **98**, 11444–11449

13 Li, B., Wei, A., Song, C., Li, N. and Zhang, J. (2008) Heterologous expression of the TsVP gene improves the drought resistance of maize. Plant Biotechnol. J. **6**, 146–159

14 Zhang, J., Li, J., Wang, X. and Chen, J. (2011) OVP1, a Vacuolar H(+)-translocating inorganic pyrophosphatase (V-PPase), overexpression improved rice cold tolerance. Plant Physiol. Biochem. **49**, 33–38

15 Asaoka, M. M. A., Segami, S., Ferjani, A. and Maeshima, M. (2016) Contribution of PP_i-hydrolyzing function of vacuolar H(+)-pyrophosphatase in vegetative growth of Arabidopsis: Evidenced by expression of uncoupling mutated enzymes. Front. Plant Sci. **7**, 415

16 Docampo, R. and Moreno, S. N. (2008) The acidocalcisome as a target for chemotherapeutic agents in protozoan parasites. Curr. Pharm. Des. **14**, 882–888

17 Shah, N.R., Vidilaseris, K., Xhaard, H. and Goldman, A. (2016) Integral membrane pyrophosphatases: a novel drug target for human pathogens? AIMS Biophys. **3**, 171–194

18 Lin, S.M., Tsai, J.Y., Hsiao, C.D., Huang, Y.T., Chiu, C.L., Liu, M.H., Tung, J.Y., Liu, T.H., Pan, R.L. and Sun, Y.J. (2012) Crystal structure of a membrane-embedded H^+-translocating pyrophosphatase. Nature **484**, 399–403

19 Kellosalo, J., Kajander, T., Kogan, K., Pokharel, K. and Goldman, A. (2012) The structure and catalytic cycle of a sodium-pumping pyrophosphatase. Science **337**, 473–476

20 Baltscheffsky, M., Schultz, A. and Baltscheffsky, H. (1999) H(+)-PPases: a tightly membrane-bound family. FEBS Lett. **457**, 527–533

21 Luoto, H.H., Nordbo, E., Malinen, A.M., Baykov, A.A. and Lahti, R. (2015) Evolutionarily

divergent, Na^+-regulated H^+-transporting membrane-bound pyrophosphatases. Biochem. J. **467**, 281–291

22 Belogurov, G.A. and Lahti, R. (2002) A lysine substitute for K^+. A460K mutation eliminates K^+ dependence in H^+-pyrophosphatase of *Carboxydothermus hydrogenoformans*. J. Biol. Chem. **277**, 49651–49654

23 Luoto, H.H., Belogurov, G.A., Baykov, A.A., Lahti, R. and Malinen, A.M. (2011) Na^+-translocating membrane pyrophosphatases are widespread in the microbial world and evolutionarily precede H^+-translocating pyrophosphatases. J. Biol. Chem. **286**, 21633–21642

24 Luoto, H.H., Baykov, A.A., Lahti, R. and Malinen, A.M. (2013) Membrane-integral pyrophosphatase subfamily capable of translocating both Na^+ and H^+. Proc. Natl. Acad. Sci. U.S.A. **110**, 1255–1260

25 Luoto, H.H., Nordbo, E., Baykov, A.A., Lahti, R. and Malinen, A.M. (2013) Membrane Na^+-pyrophosphatases can transport protons at low sodium concentrations. J. Biol. Chem. **288**, 35489–35499

26 Belogurov, G.A., Malinen, A.M., Turkina, M.V, Jalonen, U., Rytkönen, K., Baykov, A.A. and Lahti, R. (2005) Membrane-bound pyrophosphatase of *Thermotoga maritima* requires sodium for activity. Biochemistry **44**, 2088–2096

27 Bradford, M.M. (1976) A rapid and sensitive method for the quantitation of microgram quantities of protein utilizing the principle of protein-dye binding. Anal. Biochem. **72**, 248–254

28 Altschul, S.F., Gish, W., Miller, W., Myers, E.W. and Lipman, D.J. (1990) Basic local alignment search tool. J. Mol. Biol. **215**, 403–410

29 Edgar, R.C. (2004) MUSCLE: multiple sequence alignment with high accuracy and high throughput. Nucleic Acids Res. **32**, 1792–1797

30 Ronquist, F. and Huelsenbeck, J.P. (2003) MrBayes 3: Bayesian phylogenetic inference under mixed models. Bioinformatics **19**, 1572–1574

31 Baykov, A.A. and Avaeva, S.M. (1981) A simple and sensitive apparatus for continuous monitoring of orthophosphate in the presence of acid-labile compounds. Anal. Biochem **116**, 1–4

32 Malinen, A.M., Belogurov, G.A., Baykov, A.A. and Lahti, R. (2007) Na^+-pyrophosphatase: a novel primary sodium pump. Biochemistry **46**, 8872–8878

33 Casadio, R. (1991) Measurements of transmembrane pH differences of low extents in bacterial chromatophores. Eur. Biophys. J. **19**, 189–201

34 Rath, A., Glibowicka, M., Nadeau, V.G., Chen, G. and Deber, C.M. (2009) Detergent binding explains anomalous SDS-PAGE migration of membrane proteins. Proc. Natl. Acad. Sci. U.S.A. **106**, 1760–1765

35 Baykov, A.A., Dubnova, E.B., Bakuleva, N.P., Evtushenko, O.A., Zhen, R.G. and Rea, P.A. (1993) Differential sensitivity of membrane-associated pyrophosphatases to inhibition by diphosphonates and fluoride delineates two classes of enzyme. FEBS Lett. **327**, 199–202

36 Baykov, A.A., Sergina, N.V, Evtushenko, O.A. and Dubnova, E.B. (1996) Kinetic characterization of the hydrolytic activity of the H^+-pyrophosphatase of *Rhodospirillum rubrum* in membrane-bound and isolated states. Eur. J. Biochem. **236**, 121–127

37 Baykov, A.A., Bakuleva, N.P. and Rea, P.A. (1993) Steady-state kinetics of substrate hydrolysis by vacuolar H(+)-pyrophosphatase. A simple three-state model. Eur. J. Biochem. **217**, 755–762

38 Mulkidjanian, A.Y., Galperin, M.Y., Makarova, K.S., Wolf, Y.I. and Koonin, E.V. (2008) Evolutionary primacy of sodium bioenergetics. Biol. Direct **3**, 13

39 Mulkidjanian, A.Y., Galperin, M.Y. and Koonin, E.V. (2009) Co-evolution of primordial membranes and membrane proteins. Trends Biochem. Sci. **34**, 206–215

40 Leone, V., Pogoryelov, D., Meier, T. and Faraldo-Gómez, J.D. (2015) On the principle of ion selectivity in Na^+/H^+-coupled membrane proteins: experimental and theoretical studies of an ATP synthase rotor. Proc. Natl. Acad. Sci. U.S.A. **112**, E1057–1066

41 Malinen, A.M., Baykov, A.A. and Lahti, R. (2008) Mutual effects of cationic ligands and substrate on activity of the Na(+)-transporting pyrophosphatase of *Methanosarcina mazei*. Biochemistry **47**, 13447–13454

42 Gaxiola, R.A., Sanchez, C.A., Paez-Valencia, J., Ayre, B.G. and Elser, J.J. (2012) Genetic manipulation of a "vacuolar" H(+)-PPase: from salt tolerance to yield enhancement under phosphorus-deficient soils. Plant Physiol. **159**, 3–11

43 Stamatakis, A., Hoover, P. and Rougemont, J. (2008) A rapid bootstrap algorithm for the RAxML Web servers. Syst. Biol. **57**, 758–771

TABLE 1
New recombinant mPPases produced in this study

Host bacterium	DSM-No.[a]	mPPase accession number[b]	mPPase abbreviation	Notes
Brachyspira murdochii	12563	WP_013114293	Bm-PPase	
Candidatus Kuenenia stuttgartiensis	NA[c]	CAJ72581	Ks-PPase	Synthetic gene
Cytophaga fermentans	9555	WP_027472795	Cyf-PPase	Alternative name: *Saccharicrinis fermentans*
Clostridium phytofermentans	18823	WP_012199835	Cp-PPase	Cloned into pET15b. Alternative name: *Lachnoclostridium phytofermentans*
Dehalogenimonas lykanthroporepellens	NA	ADJ26073.1	Dl-PPase	Synthetic gene
Mahella australiensis	15567	AEE96015.1	Ma-PPase	
Melioribacter roseus	23840	WP_014857027	Mr-PPase	
Methylomonas methanica	25384	AEG00770.1	Mme-PPase	
Oscillibacter valericigenes	18026	WP_014119890	Ov-PPase	
Shuttleworthia satelles	14600	WP_006906218	Ss-PPase	

[a] Accession number of the mPPase host organism at Leibniz-Institute DSMZ (Deutsche Sammlung von Microorganismen und Zellkulturen GmbH)
[b] NCBI GenBank accession number of mPPase protein sequence
[c] NA, not applicable

TABLE 2
Fitted parameter values ± SE for Eq. 1 describing effects of alkali cations on mPPase activity in Figure 3

mPPase	V_1, μmol·min^{-1}·mg^{-1}		K_a, mM		K_i, mM		V_{+K}/V_{-K}
	-K^+	+K^+	-K^+	+K^+	-K^+	+K^+	
Bm	0.19 ± 0.01	0.28 ± 0.02	34 ± 6	0.16 ± 0.03	180 ± 40	85 ± 50	1.5
Dl	0.104 ± 0.005	0.43 ± 0.03	36 ± 7	1.0 ± 0.2	NA[a]	500 ± 400	4.1
Ks	0.19 ± 0.01	0.55 ± 0.01	28 ± 6	1.00 ± 0.08	NA	NA	2.9
Mme	0.070 ± 0.002	0.23 ± 0.01	54 ± 4	1.0 ± 0.3	NA	250 ± 100	3.3
Ov	0.26 ± 0.03	0.47 ± 0.02	15 ± 4	0.11 ± 0.02	400 ± 200	24 ± 8	1.8
Ss	0.17 ± 0.02	0.24 ± 0.01	40 ± 9	0.22 ± 0.06	160 ± 40	45 ± 35	1.4
Mr	0.118 ± 0.004	0.26 ± 0.02	24 ± 3	0.8 ± 0.2	NA	280 ± 200	2.2
Cyf	0.069 ± 0.003	0.22 ± 0.01	30 ± 5	1.6 ± 0.2	NA	250 ± 90	3.2
Ma[b]	0.078 ± 0.006	0.057 ± 0.006	17 ± 3	0.106 ± 0.03	180 ± 40	218 ± 70	0.7
Cp	0.018 ± 0.001	0.056 ± 0.006	14 ± 4	0.11 ± 0.04	NA	80 ± 40	3.1

[a] NA, not applicable
[b] Assuming $V_2 = 0$ both in the absence and presence of K^+

FIGURE LEGENDS

Figure 1 Phylogeny of membrane-bound PPase protein sequences as determined with MrBayes.
(A) A complete phylogenetic tree of the mPPase protein superfamily [21]. Different subfamilies are depicted by color coding. *M. mazei* Na^+-PPase is marked as M. (B) Detailed phylogeny at the interface of Na^+-PPases and Na^+,H^+-PPases. The tree was rooted at *Waddlia chondrophila* mPPase (marked as W on panel A) that is an outgroup taxon relative to the investigated Na^+-PPases and Na^+,H^+-PPases. The numbers refer to clade credibility values, however those ≥90 are not shown for clarity. The clades supported with ≤50 credibility values are drawn as polytomies. The enzymes investigated in this study are indicated in bold; previously characterized Na^+,H^+-PPases [24] are marked with an asterisk. The borders of Na^+-PPase (indicated with a purple background color), Na^+-regulated Na^+,H^+-PPase (orange) and true Na^+,H^+-PPase (pink) subfamilies were predicted based on the experimental data presented in this study and tree topology. The subfamilies of taxa on a white background could not be reasonably predicted. Scale bars in both figures represent 0.2 amino acid substitutions per residue.

Figure 2 Expression of enzymatically active recombinant mPPases in *E. coli*.
(A) Western analysis of IMVs prepared from C41(DE3) cells transformed with mPPase expression constructs or vector only. IMVs (10 μg total protein) were subjected to SDS-PAGE, electrotransferred, and probed with anti-mPPase primary antibody and fluorescently labeled (IRDye 800CW, Li-Cor) anti-rabbit secondary antibody. Loading order and molecular masses (in kDa) predicted from the sequence: lane 1, molecular mass markers; lane 2, Mr-PPase (76); lane 3, Cyf-PPase (79); lane 4, Ks-PPase (84); lane 5, Bm-PPase (83); lane 6, Ma-PPase (73); lane 7, Cp-PPase (72); lane 8, Ss-PPase (72); lane 9, Ov-PPase (71); lane 10, Mme-PPase (71); lane 11, Dl-PPase (70); lane 12, authentic *E. coli* IMVs. (B) The protein content of the IMVs used for panel A was visualized by Coomassie staining of SDS-PAGE gels. The IMV samples (10 μg total protein) were loaded in the same order as in panel A. The expected region of mPPase bands is indicated on the right. (C) PP_i hydrolysis activities of the IMVs. Where indicated, 250 μM potassium fluoride (inhibitor of soluble *E. coli* PPase) or 20 μM AMDP (inhibitor of mPPases) was included in the reaction buffer. Error bars represent SD of three separate measurements.

Figure 3 Dependence of the mPPase-catalyzed PP_i hydrolysis reaction on alkali metal ions.
The K^+ concentration was either zero or 50 mM. Lines were obtained from Eq. 1 using the best-fit parameter values in Table 2.

Figure 4 Na^+-transport activity of mPPases.
Na^+ accumulation inside IMVs was measured after a 1-min incubation with or without TMA_4-PP_i. Error bars indicate SD of three independent measurements. Lb-PPase and Cl-PPase have previously been characterized as H^+-PPases and Na^+-PPases, respectively [23].

Figure 5 Na^+ concentration dependence of mPPase-catalyzed H^+ transport into IMVs, as reported by ACMA fluorescence.
The H^+-transport reaction was initiated by adding 475 μM TMA-PP_i at approximately the 2-min time point and was reversed by adding 10 mM ammonium chloride (at ~7 min) to collapse the steady-state proton gradient. The IMV concentration was 0.15 mg ml^{-1}, except for Am-, Cle- and Po-PPase, which were used at 0.30 mg ml^{-1} concentration owing to their low PP_i hydrolysis activities (<0.05 μmol min^{-1} mg^{-1}). The asterisk indicates previously characterized Na^+,H^+-PPases [24]. The colored square following the enzyme name in each panel indicates the subfamily to which the particular mPPase was attributed (same colors as in Figure 1B).

Figure 1

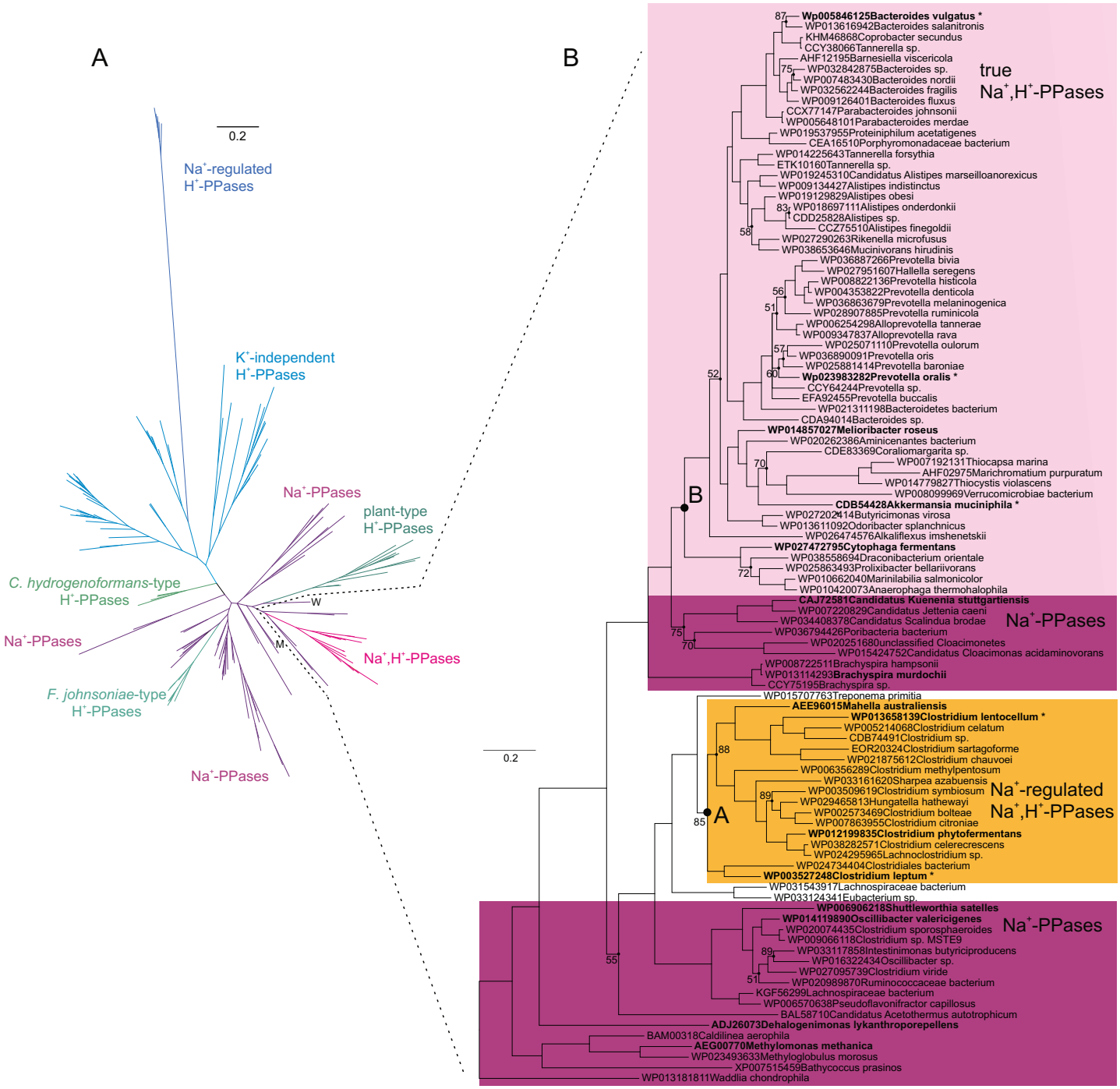
A
0.2
Na+-regulated H+-PPases
K+-independent H+-PPases
Na+-PPases
plant-type H+-PPases
C. hydrogenoformans-type H+-PPases
Na+-PPases
Na+,H+-PPases
F. johnsoniae-type H+-PPases
Na+-PPases
W
M
B
0.2
true Na+,H+-PPases
Na+-PPases
Na+-regulated Na+,H+-PPases
Na+-PPases
A
B
Wp005846125Bacteroides vulgatus *
WP013616942Bacteroides salanitronis
KHM46868Coprobacter secundus
CCY38066Tannerella sp.
AHF12195Barnesiella viscericola
WP032842875Bacteroides sp.
WP007483430Bacteroides nordii
WP032562244Bacteroides fragilis
WP009126401Bacteroides fluxus
CCX77147Parabacteroides johnsonii
WP005648101Parabacteroides merdae
WP019537955Proteiniphilum acetatigenes
CEA16510Porphyromonadaceae bacterium
WP014225643Tannerella forsythia
ETK10160Tannerella sp.
WP019245310Candidatus Alistipes marseilloanorexicus
WP009134427Alistipes indistinctus
WP019129829Alistipes obesi
WP018697111Alistipes onderdonkii
CDD25828Alistipes sp.
CCZ75510Alistipes finegoldii
WP027290263Rikenella microfusus
WP038653646Mucinivorans hirudinis
WP036887266Prevotella bivia
WP027951607Hallella seregens
WP008822136Prevotella histicola
WP004353822Prevotella denticola
WP036863679Prevotella melaninogenica
WP028907885Prevotella ruminicola
WP006254298Alloprevotella tannerae
WP009347837Alloprevotella rava
WP025071110Prevotella oulorum
WP036890091Prevotella oris
WP025881414Prevotella baroniae
Wp023983282Prevotella oralis *
CCY64244Prevotella sp.
EFA92455Prevotella buccalis
WP021311198Bacteroidetes bacterium
CDA94014Bacteroides sp.
WP014857027Melioribacter roseus
WP020262386Aminicenantes bacterium
CDE83369Coraliomargarita sp.
WP007192131Thiocapsa marina
AHF02975Marichromatium purpuratum
WP014779827Thiocystis violascens
WP008099969Verrucomicrobiae bacterium
CDB54428Akkermansia muciniphila *
WP027202414Butyricimonas virosa
WP013611092Odoribacter splanchnicus
WP026474576Alkaliflexus imshenetskii
WP027472795Cytophaga fermentans
WP038558694Draconibacterium orientale
WP025863493Prolixibacter bellariivorans
WP010662040Marinilabilia salmonicolor
WP010420073Anaerophaga thermohalophila
CAJ72581Candidatus Kuenenia stuttgartiensis
WP007220829Candidatus Jettenia caeni
WP034408378Candidatus Scalindua brodae
WP036794426Poribacteria bacterium
WP020251680unclassified Cloacimonetes
WP015424752Candidatus Cloacimonas acidaminovorans
WP008722511Brachyspira hampsonii
WP013114293Brachyspira murdochii
CCY75195Brachyspira sp.
WP015707763Treponema primitia
AEE96015Mahella australiensis
WP013658139Clostridium lentocellum *
WP005214068Clostridium celatum
CDB74491Clostridium sp.
EOR20324Clostridium sartagoforme
WP021875612Clostridium chauvoei
WP006356289Clostridium methylpentosum
WP033161620Sharpea azabuensis
WP003509619Clostridium symbiosum
WP029465813Hungatella hathewayi
WP002573469Clostridium bolteae
WP007863955Clostridium citroniae
WP012199835Clostridium phytofermentans
WP038282571Clostridium celerecrescens
WP024295965Lachnoclostridium sp.
WP024734404Clostridiales bacterium
WP003527248Clostridium leptum *
WP031543917Lachnospiraceae bacterium
WP033124341Eubacterium sp.
WP006906218Shuttleworthia satelles
WP014119890Oscillibacter valericigenes
WP020074435Clostridium sporosphaeroides
WP009066118Clostridium sp. MSTE9
WP033117858Intestinimonas butyriciproducens
WP016322434Oscillibacter sp.
WP027095739Clostridium viride
WP020989870Ruminococcaceae bacterium
KGF56299Lachnospiraceae bacterium
WP006570638Pseudoflavonifractor capillosus
BAL58710Candidatus Acetothermus autotrophicum
ADJ26073Dehalogenimonas lykanthroporepellens
BAM00318Caldilinea aerophila
AEG00770Methylomonas methanica
WP023493633Methyloglobulus morosus
XP007515459Bathycoccus prasinos
WP013181811Waddlia chondrophila

Figure 2

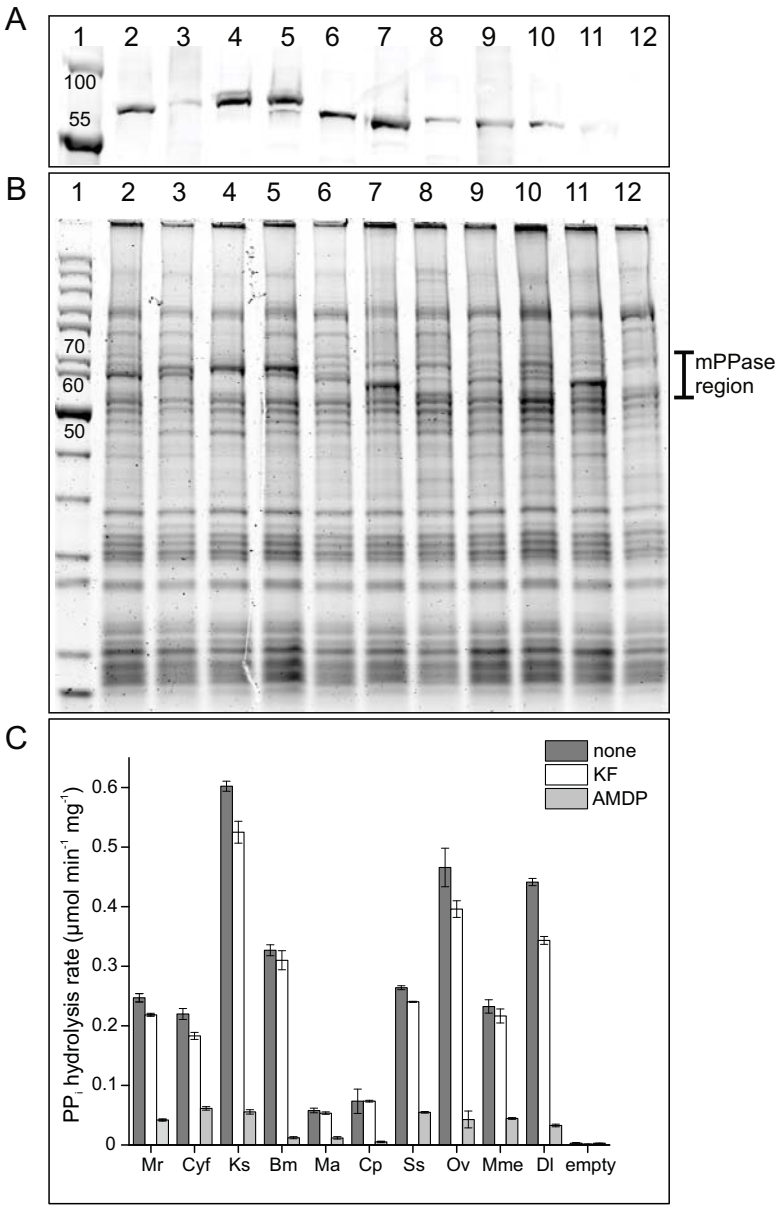
A
1 2 3 4 5 6 7 8 9 10 11 12
100
55
B
1 2 3 4 5 6 7 8 9 10 11 12
70
60
50
mPPase region
C
none
KF
AMDP
PPi hydrolysis rate (μmol min-1 mg-1)
0
0.1
0.2
0.3
0.4
0.5
0.6
Mr Cyf Ks Bm Ma Cp Ss Ov Mme Dl empty

Figure 3

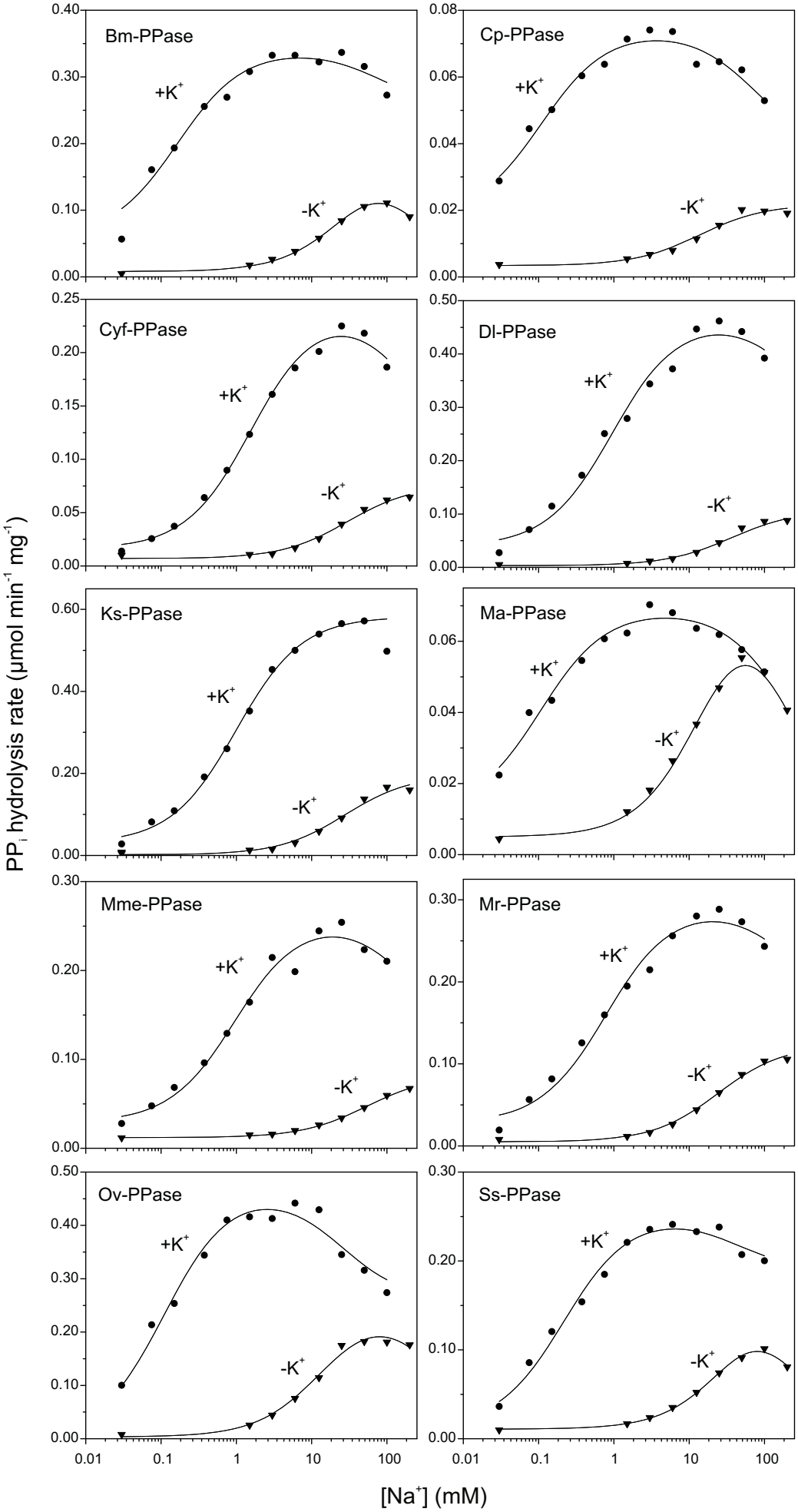
Bm-PPase
Cp-PPase
Cyf-PPase
Dl-PPase
Ks-PPase
Ma-PPase
Mme-PPase
Mr-PPase
Ov-PPase
Ss-PPase
+K+
-K+
PPi hydrolysis rate (μmol min-1 mg-1)
[Na+] (mM)

Figure 4

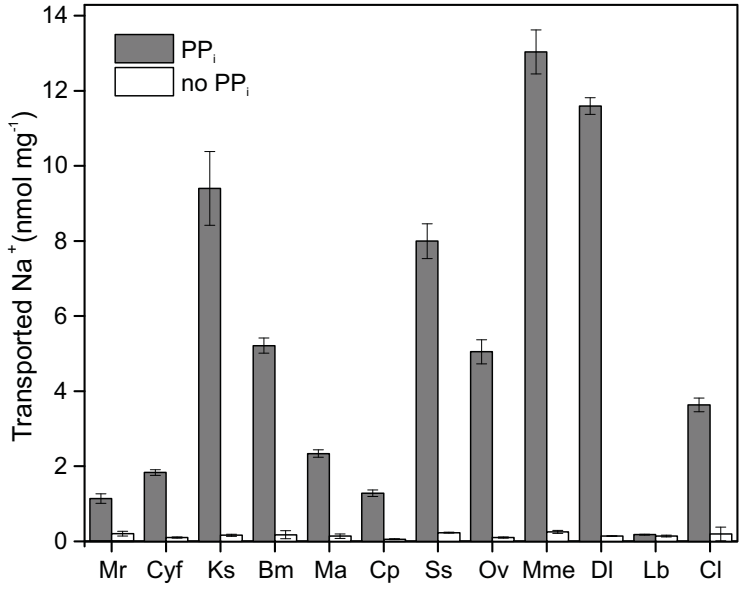
PPi
no PPi
Transported Na+ (nmol mg-1)
0
2
4
6
8
10
12
14
Mr
Cyf
Ks
Bm
Ma
Cp
Ss
Ov
Mme
Dl
Lb
Cl

Figure 5

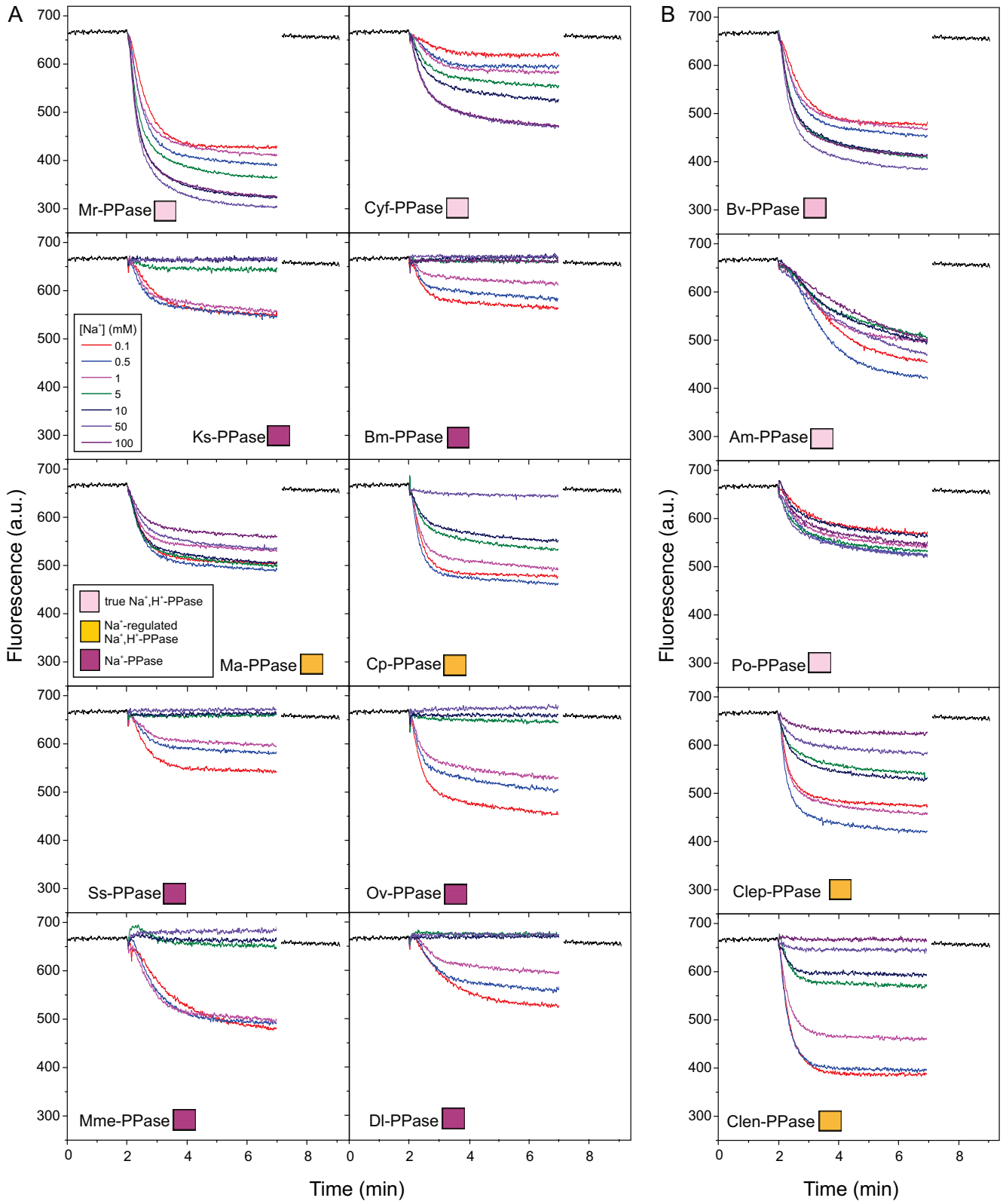
A
B
Fluorescence (a.u.)
Time (min)
[Na+] (mM)
0.1
0.5
1
5
10
50
100
true Na+,H+-PPase
Na+-regulated Na+,H+-PPase
Na+-PPase
Mr-PPase
Cyf-PPase
Ks-PPase
Bm-PPase
Ma-PPase
Cp-PPase
Ss-PPase
Ov-PPase
Mme-PPase
Dl-PPase
Bv-PPase
Am-PPase
Po-PPase
Clep-PPase
Clen-PPase

SUPPLEMENTARY MATERIAL

Two independent evolutionary routes to Na^+/H^+ co-transport function in membrane pyrophosphatases

Erika Nordbo*, Heidi H. Luoto*, Alexander A. Baykov†, Reijo Lahti* and Anssi M. Malinen*

*Department of Biochemistry, University of Turku, FIN-20014 Turku, Finland.
†Belozersky Institute of Physico-Chemical Biology, Lomonosov Moscow State University, Moscow 119899, Russia.

Supplementary Figure 1

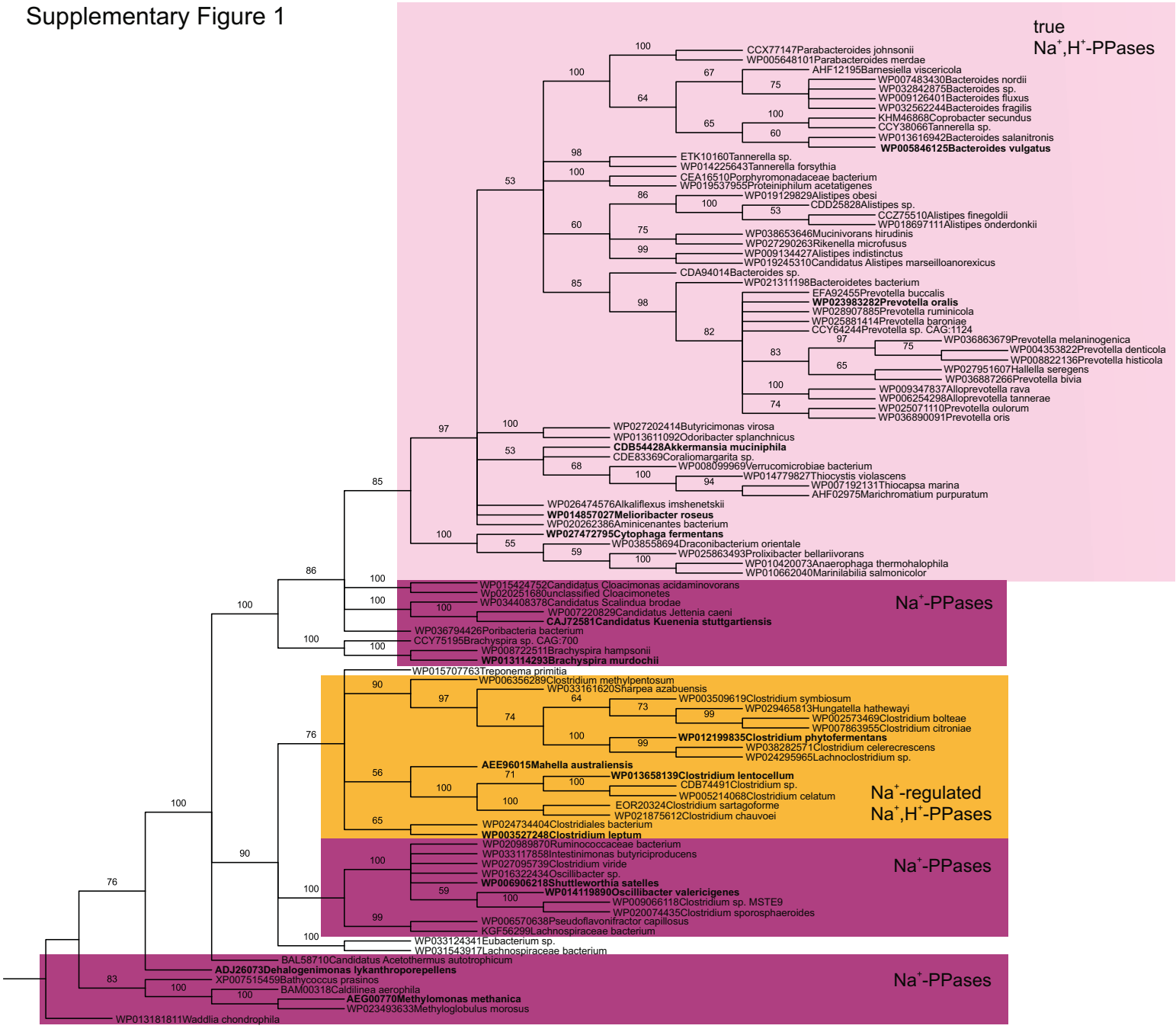

Figure S1 Phylogeny at the interface of Na^+-PPases and Na^+,H^+-PPases predicted with a different software. The majority rule consensus tree was calculated with the RAxML web-server (http://embnet.vital-it.ch/raxml-bb/) [43] using default settings and the same sequence block as for the tree in Figure 1B. The enzymes investigated in this study are indicated by their abbreviated names; previously characterized Na^+,H^+-PPases [24] are additionally marked with an asterisk. Different subfamilies are depicted by color coding. The tree was rooted at *W. chondrophila* mPPase. The clades supported with bootstrap values $\leqslant 50$ are drawn as polytomies.

24 Luoto, H.H., Baykov, A.A., Lahti, R. and Malinen, A.M. (2013) Membrane-integral pyrophosphatase subfamily capable of translocating both Na^+ and H^+. Proc. Natl. Acad. Sci. U.S.A. **110**, 1255–1260

43 Stamatakis, A., Hoover, P. and Rougemont, J. (2008) A rapid bootstrap algorithm for the RAxML Web servers. Syst. Biol. **57**, 758–771